

## Phase diagram of the $U(2) \times U(2)$ scalar model in three dimensions

---

**Kazuhiko Kamikado\***

*Theoretical Research Division, Nishina Center, RIKEN, Wako, Saitama 351-0198, Japan*

*E-mail: [kazuhiko.kamikado@riken.jp](mailto:kazuhiko.kamikado@riken.jp)*

We investigate phase transitions of the  $U(2) \times U(2)$  scalar model as a chiral effective model of 2-flavor QCD. In order to evaluate observables, we discretize the  $U(2) \times U(2)$  scalar model on three dimensional lattice and perform the hybrid Monte Carlo simulation. We present a phase diagram in the parameter space and show the order of the phase transition of the model strongly depends on the model parameter. We discuss a relation between the phase structure and the renormalization group flow.

*The 33rd International Symposium on Lattice Field Theory  
14 -18 July 2015  
Kobe International Conference Center, Kobe, Japan*

---

\*Speaker.

## 1. Introduction

Restoration of the chiral symmetry is one of the important characteristics of quantum chromodynamics (QCD) at finite temperature. The chiral symmetry of QCD is spontaneously broken at low temperature while it is restored at high temperature. The nature of the chiral phase transition is extensively investigated by the lattice QCD or chiral effective models, for review [1].

The  $U(2) \times U(2)$  scalar model is one of the chiral effective models introduced by Pisarski and Wilczek [2]. If the  $U_A(1)$  anomaly is effectively restored at the critical temperature, the chiral phase transition of 2-flavor QCD is described by the  $U(2) \times U(2)$  scalar model. Pisarski and Wilczek have calculated the one-loop beta functions of the renormalization group (RG) and they have shown that there is no infra red (IR) fixed point of the beta functions which corresponds to the chiral phase transition. Therefore they concluded that the order of the chiral phase transition of 2-flavor QCD is of first order. After Pisarski and Wilczek's work, the possibility of a second order phase transition has been investigated by many theoretical frameworks, such as, higher order perturbation theory [3, 4], the functional renormalization group [5, 6, 7] and the conformal bootstrap method [8]. Because the existence of the IR fixed point of the RG flow strongly depends on the frameworks or the approximations, the order of the chiral phase transition of the model is still unclear.

In this paper, we discretise the  $U(2) \times U(2)$  scalar model on three dimensional lattice and perform the hybrid Monte Carlo simulation. We observe the order parameter and its Binder cumulant near the phase boundary and determine the order of the chiral phase transition. These analyses is carried out in a wide range of the parameter space of the model and we present the phase diagram of the model.

## 2. Formalism

### 2.1 $U(2) \times U(2)$ scalar model

The Lagrangian of the  $U(2) \times U(2)$  scalar model is as follows:

$$\mathcal{L} = \frac{1}{2} \text{tr}(\partial_\mu \Phi^\dagger \partial_\mu \Phi) + \frac{1}{2} \mu^2 \text{tr} \Phi^\dagger \Phi + \frac{g_1}{4} (\text{tr} \Phi^\dagger \Phi)^2 + \frac{g_2}{4} \text{tr} (\Phi^\dagger \Phi)^2, \quad (2.1)$$

where  $\Phi$  is a complex  $2 \times 2$  matrix. The Lagrangian is invariant under the transformation,

$$\Phi \rightarrow U_L \Phi U_R^\dagger \quad (2.2)$$

where  $U_L$  and  $U_R$  are independent  $U(2)$  matrices. It is more convenient to parameterise the matrix  $\Phi$  in terms of the scalar and pseud-scalar mesons as

$$\Phi = \Sigma + i\Pi = \sum_{i=0}^{i=3} t_a (\sigma_i + i\pi_a), \quad (2.3)$$

where  $t_a$  is the  $U(2)$  generators normalized  $\text{tr}[t_a t_b] = \delta_{ab}$ . We can write

$$\begin{aligned} \Sigma &= \begin{pmatrix} \frac{1}{\sqrt{2}} a^0 + \frac{1}{\sqrt{2}} \sigma & a^+ \\ a^- & -\frac{1}{\sqrt{2}} a^0 + \frac{1}{\sqrt{2}} \sigma \end{pmatrix} \\ \Pi &= \begin{pmatrix} \frac{1}{\sqrt{2}} \pi^0 + \frac{1}{\sqrt{2}} \eta & \pi^+ \\ \pi^- & -\frac{1}{\sqrt{2}} \pi^0 + \frac{1}{\sqrt{2}} \eta \end{pmatrix}, \end{aligned} \quad (2.4)$$

where  $a^\pm = (a_1 \mp ia_2)$  and  $\pi^\pm = (\pi_1 \mp i\pi_2)$ . We can rewrite the Lagrangian in terms of mesons,

$$L = \frac{1}{2} [(\partial_\mu \sigma)^2 + (\partial_\mu \vec{\pi})^2 + (\partial_\mu \eta)^2 + (\partial_\mu \vec{a})^2] + \frac{1}{2} \mu^2 (\sigma^2 + \vec{\pi}^2 + \eta^2 + \vec{a}^2) \\ + \frac{g_1 + \frac{1}{2}g_2}{4} (\sigma^2 + \vec{\pi}^2 + \eta^2 + \vec{a}^2)^2 + \frac{2g_2}{4} ((\sigma^2 + \vec{\pi}^2)(\eta^2 + \vec{a}^2) - (\sigma\eta - \vec{\pi}\vec{a})^2). \quad (2.5)$$

The stable conditions for the classical potential are

$$g_1 + g_2 > 0, \\ g_1 + \frac{1}{2}g_2 > 0. \quad (2.6)$$

In this paper, we only consider  $g_2 > 0$ , therefore, the first condition is always satisfied if we care the second one. In this case, the model shares the same symmetry breaking pattern with 2-flavor QCD without  $U_A(1)$  anomaly, that is  $U_V(2) \times U_A(2) \rightarrow U_V(2)$ . The symmetry breaking pattern implies that there appear four Nambu-Goldstone modes in the broken phase.

## 2.2 Hybrid Monte Carlo method

In this paper, we consider the  $U(2) \times U(2)$  scalar model on three dimensional lattice. We consider a simple cubic lattice with a lattice unit “ $a$ ” and lattice size “ $L$ ”. The action of the model is

$$S = a^3 \sum_{x, \hat{\mu}} \frac{1}{2a^2} \text{tr}(\Phi_{x+\hat{\mu}}^\dagger - \Phi_x^\dagger)(\Phi_{x+\hat{\mu}} - \Phi_x) \\ + a^3 \sum_x \left( \frac{\mu^2}{2} \text{tr}(\Phi_x^\dagger \Phi_x) + \frac{g_1}{4} (\text{tr}(\Phi_x^\dagger \Phi_x))^2 + \frac{g_2}{4} \text{tr}(\Phi_x^\dagger \Phi_x \Phi_x^\dagger \Phi_x) \right), \quad (2.7)$$

where the sum of  $x$  runs over all lattice sites and the sum of  $\hat{\mu}$  is taken for a unit lattice size and positive direction. In the following, we only consider the lattice spacing is unity  $a = 1$  case and omit  $a$ .

In order to evaluate observables, we utilize the hybrid Monte Carlo method. The hybrid Monte Carlo method is performed under the following procedure. For simplicity, we consider an action composed of a scalar field( $\phi$ ):  $S[\phi] = \int dx^d L[\phi]$ . From the action, we can compute an expectation value of an operator  $O[\phi]$  as,

$$\langle O[\phi] \rangle = \int [d\phi] O[\phi] e^{-S[\phi]}. \quad (2.8)$$

Instead of performing the path integral exactly, we make a sampling by utilizing the hybrid Monte Carlo method. First we generate the canonical momentum ( $\pi$ ) of the scalar field with the following probability:

$$p(\pi) \propto e^{-\frac{1}{2}\pi^2}. \quad (2.9)$$

The evolution of  $\phi$  and  $\pi$  to the Monte-Carlo time ( $\tau$ ) is described the following equation,

$$\partial_\tau \phi = \frac{\partial H}{\partial \pi} = \pi \\ \partial_\tau \pi = -\frac{\partial H}{\partial \phi}, \quad (2.10)$$

with the Hamiltonian,

$$H \equiv \frac{1}{2} \pi^2 + S[\phi]. \quad (2.11)$$

We can solve the above evolution with the Leap-frog method. At every predetermined interval, we make a Metropolis accept/reject check with a probability,

$$P(\Delta H) = \min \{1, e^{-\Delta H}\}, \quad (2.12)$$

where  $\Delta H$  is a difference of the energy from the previous Metropolis check. If  $\Delta H < 0$ , the configuration is always approved. If  $\Delta H > 0$ , the configuration is approved with the probability  $P = e^{-\Delta H}$ . If the configuration is rejected, we restore the configuration to the configuration at the previous Metropolis check. The canonical momentum  $\pi$  is generated at each Metropolis check. Because the HMC program satisfies the detailed balance condition and then the expectation values of observable are calculated by

$$\langle O[\phi] \rangle = \frac{1}{N} \sum_{n=1, \dots, N} O[\phi_n], \quad (2.13)$$

where the index  $n$  indicates the order of the Metropolis check.

There are two adjustable parameters in the hybrid Monte Carlo simulation, the number of leapfrog steps ( $N$ ) and the step size ( $\epsilon$ ). We adjust the step size to keep the acceptance rate  $80 \sim 90$  % in each simulation. We also set the number of leapfrog steps as  $\epsilon N \sim 1.0$ .

### 2.3 Observables

We use magnetization as an order parameter,

$$\text{Magnetization} : M \equiv \left\langle (\text{tr} \bar{\Phi}^\dagger \bar{\Phi})^{1/2} \right\rangle \quad (2.14)$$

where  $\bar{\Phi}$  is a normalized matrix field and defined as

$$\bar{\Phi} \equiv \sum_x \Phi_x / L^3. \quad (2.15)$$

In the thermodynamic limit ( $L \rightarrow \infty$ ), the magnetization has finite value in the broken phase while it is zero in the symmetric phase. In order to distinguish the order of the phase transition, the Binder cumulant is useful:

$$\text{Binder cumulant} : U_L \equiv 1 - \frac{\left\langle (\text{tr} \bar{\Phi}^\dagger \bar{\Phi})^2 \right\rangle}{3 \left\langle \text{tr} \bar{\Phi}^\dagger \bar{\Phi} \right\rangle^2}. \quad (2.16)$$

In the thermodynamic limit, the Binder cumulant coincide  $2/3$  in the symmetry breaking phase, while in the symmetric phase, it takes a value smaller than  $2/3$ . At finite lattice size the Binder cumulant becomes independent to the volume of the system at the second order phase boundary.

### 3. Results

In this section, we present numerical results of our simulation. In order to determine the phase structure, we observe the observables in the parameter space  $\mu^2$ ,  $g_1$ ,  $g_2$ . For small  $\mu^2$ , the spontaneously symmetry breaking phase realizes, while the symmetric phase appears for large  $\mu^2$ . Near the phase boundary, we carefully evaluated the magnetization and Binder cumulant and determine the order of the phase transition. In all simulation, the statistical error of the simulation is evaluated by the jackknife technique.

## Second order

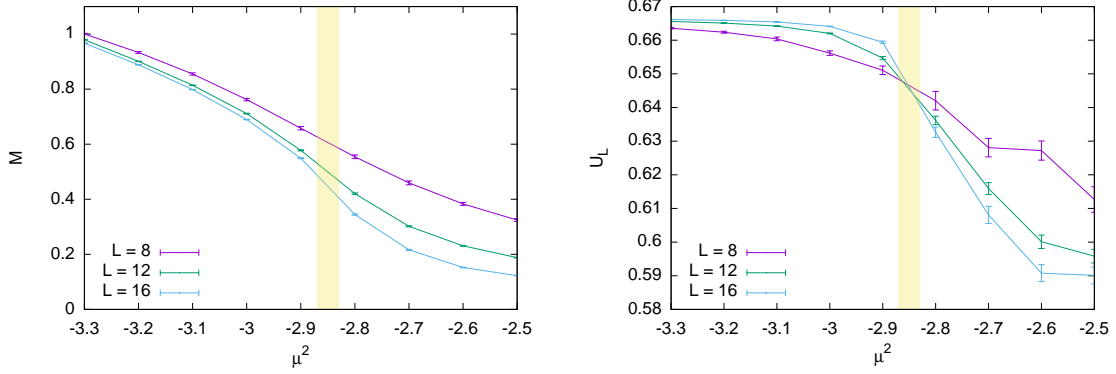


**Figure 1:** Magnetization and Binder cumulant near the second order critical coupling ( $g_1 = 0.5$ ,  $g_2 = 1.0$ ). The yellow band indicates the estimated critical coupling.

We start the simulation from positive  $g_1$ . In this parameter region, the model shows second order phase transition. Left panel of fig. 1 shows the volume dependence of the magnetization near a phase boundary ( $g_1 = 0.5$ ,  $g_2 = 1.0$ ). We have evaluated the magnetization for  $L = 8, 12$  and  $16$ . Yellow band in the figure indicates an estimated critical coupling  $\mu^{2*} \sim -2.87$ . For  $\mu^2$  larger than  $\mu^{2*}$ , the magnetization has a finite expectation value. At  $\mu^2 > 3.0$ , the volume dependence of the magnetization is weak and the magnetization looks to converge at  $L = 16$ . Below  $\mu^{2*}$ , the magnetization decreases with increasing the lattice size. In the symmetric phase, the magnetization should converge to zero at  $L \rightarrow \infty$ . In this region  $L = 16$  is not enough for the thermodynamic limit.

In order to make sure the order of the phase transition, we evaluate the Binder cumulant near the critical coupling. The Binder cumulant for  $L = 8, 12, 16$  is shown in the right panel of fig. 1. Near the phase boundary, the Binder cumulant becomes volume independent with the critical Binder cumulant  $U_L \sim 0.645$ . This behavior of the Binder cumulant is typical in a system undergoes the second order phase transition. Therefore we can regard the phase transition of the  $U(2) \times U(2)$  scalar model at this coupling is of second order.

## First order

Next we perform the simulation at relatively smaller  $g_1$ , ( $= -0.4$ ). Left panel of fig. 2 shows the volume dependence of the magnetization near the critical coupling. The behavior of the magnetization at this parameter is completely different from that of the previous parameter. Near the critical coupling  $\mu^{2*} \sim -0.78$ , the magnetization jumps. This is a typical behavior of a system exhibit a first order phase transition. Right panel of fig. 2 displays the histogram of the magnetization for  $L = 16$  near the critical coupling. We recognize a double peak structure of the histogram. This is also a characteristic behavior of the system undergoes first order phase transition. The double peak structure appears very narrow  $\mu^2$  region and it disappears at  $\mu^2 = -0.77$ . From these observations, we can regard the phase transition of the  $U(2) \times U(2)$  scalar model at this coupling is of first order.

## Phase diagram

Finally we make the same simulation in the wide range of the parameter space and determine

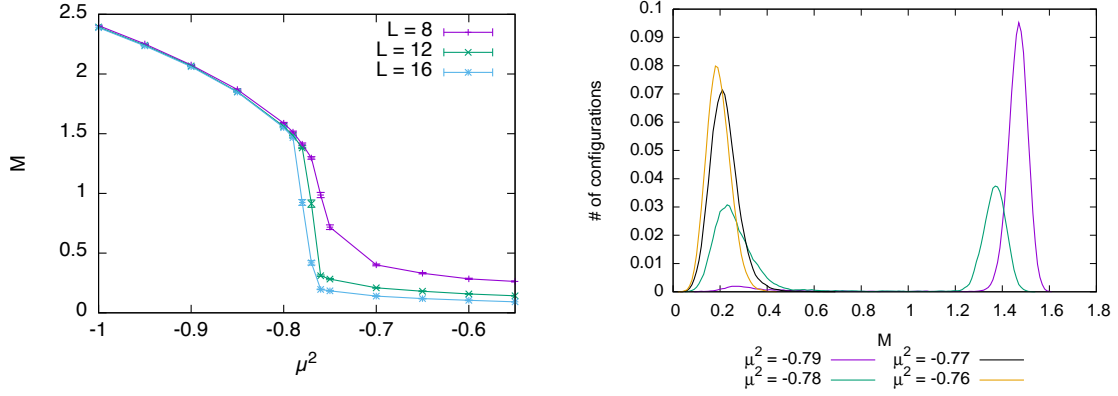


**Figure 2:** Left: Volume dependence of the magnetization near 1st order critical coupling ( $g_1 = -0.4$ ,  $g_2 = 1.0$ ). Right: Histogram of the magnetization for  $L = 16$ .

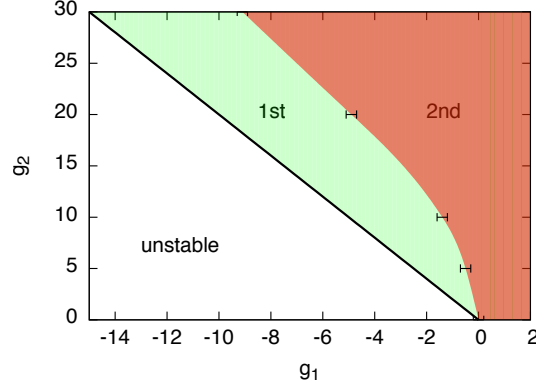


**Figure 3:** Order of phase transition of  $U(2) \times U(2)$  scalar model in 3 dimension.

the phase diagram of the  $U(2) \times U(2)$  scalar model. Fig. 3 displays the phase diagram of the  $U(2) \times U(2)$  scalar model. In the region where  $g_1 + g_2/2 < 0$ , the potential is unstable and the expectation values of the observables are not defined. In the green region, the system undergoes the first order phase boundary. We have distinguished the region by the emergence of the double peak structure of the histogram for  $L = 16$ . If we increase  $g_1$ , the interval of the two peaks becomes narrow and at some the two peaks merge together. We determine the phase boundary of the first and second order region as the point that the double peak structure disappears. Because the interval of the two peaks becomes very narrow near the phase boundary, the precise determination of the phase boundary is difficult. We expect that the value of the phase boundary contains an error at least  $\pm 0.1$  to  $g_1$  direction (indicated as error bars in the figure).

The structure of the phase diagram implies the existence of the  $U(2) \times U(2)$  IR fixed point of the RG flow [4]. The region in which the system undergoes the second order phase transition corresponds to the attraction domain of the RG flow flowing into the  $U(2) \times U(2)$  fixed point. On the other hand, the region in which the system undergoes the first order phase transition is a region where the RG flow emerges from the IR fixed point. Since the order of the phase transition depends

on the model parameter, in order to determine the order of the chiral phase transition of the 2-flavor QCD, we need to precisely determine the value of the model parameter from physical observables.

#### 4. Conclusion

We have discussed the chiral phase transition of 2-flavor QCD without  $U_A(1)$  anomaly. In order to determine the order of chiral phase transition, we performed the hybrid Monte Carlo simulation of the  $U(2) \times U(2)$  scalar model on three dimensional lattice.

We found that the order of the phase transition of the model strongly depends on the value of the model parameter. For large 4th order parameter of the model, the system undergoes second order phase transition. This fact indicates the existence of the infrared fixed point of the RG flow which belongs to the  $U(2) \times U(2)$  universality class. However this does not mean the chiral phase transition is always of second order. In deed, if we decrease the 4th order parameter, the phase transition changes to of first order. We need to fix the model parameter of the model, in order to determine the order of the chiral phase transition of 2-flavor QCD.

#### Acknowledgments

The author would like to thank T. Hatsuda, W. Weise, T. Kanazawa and Y. Tanizaki for useful discussions. K. K. was supported by the Special Postdoctoral Research Program of RIKEN.

#### References

- [1] K. Fukushima and T. Hatsuda, Rept. Prog. Phys. **74**, 014001 (2011) [arXiv:1005.4814 [hep-ph]].
- [2] R. D. Pisarski and F. Wilczek, Phys. Rev. D **29**, 338 (1984).
- [3] A. Butti, A. Pelissetto and E. Vicari, JHEP **0308**, 029 (2003) [hep-ph/0307036].
- [4] A. Pelissetto and E. Vicari, Phys. Rev. D **88**, no. 10, 105018 (2013) [arXiv:1309.5446 [hep-lat]].
- [5] J. Berges, N. Tetradis and C. Wetterich, Phys. Rept. **363**, 223 (2002) [hep-ph/0005122].
- [6] K. Fukushima, K. Kamikado and B. Klein, Phys. Rev. D **83**, 116005 (2011) [arXiv:1010.6226 [hep-ph]].
- [7] M. Grahl, Phys. Rev. D **90**, no. 11, 117904 (2014) [arXiv:1410.0985 [hep-th]].
- [8] Y. Nakayama and T. Ohtsuki, Phys. Rev. D **91**, no. 2, 021901 (2015) [arXiv:1407.6195 [hep-th]].